Design and Characterization of a Bearingless Cross-Flow Fan

I. Bagaric,
D. Steinert,
F. Wassmer,
T. Holenstein,
T. Nussbaumer,
J. W. Kolar

Design and Characterization of a Bearingless Cross-Flow Fan

Ivana Bagaric*, Daniel Steinert†, Florian Wassmer†, Thomas Holenstein†,
Thomas Nussbaumer† and Johann W. Kolar*
*Power Electronic Systems Laboratory, ETH Zurich, Switzerland, bagaric@lem.ee.ethz.ch
†Levitronix GmbH, Zurich, Switzerland, steinert@levitronix.com

Abstract—This paper presents a high-speed bearingless cross-flow fan particularly suited for applications in chemically demanding environments. In general, bearingless motors convince with a friction- and wear-free operation, unlimited lifetime and a hermetically-sealed encapsulation of the rotor. For the proposed cross-flow fan, a double-sided use of such motors additionally leads to twice the available torque for the blade rotation as well as a highly compact and safe system design. In sophisticated applications (e.g. gas-circulation systems of excimer laser) those arguments are crucial. After a description of the motor topology, the novel bearingless cross-flow fan prototype is introduced. To characterize its performance, measurements are performed on a ISO 5801 based test rig.

Fig. 1: Introduced cross-flow fan composed of two bearingless motors, two magnets and cross-flow fan blades.

I. INTRODUCTION

Bearingless motors enable a fully contactless magnetic levitation of rotors because of their integrated bearing and drive functionality [1]. The various types of bearingless motors share the same convincing advantages of long lifetime and low maintenance costs, since they allow friction- and wear-free operation [2]. Moreover, a large air gap design between stator and rotor makes a hermetically-sealed encapsulation of the rotor possible. The stator can then operate the completely separated and isolated rotor in chemically demanding, high-purity or extreme temperature environments [3]. Those advantages of bearingless motors improve many demanding systems for example in the semiconductor, pharmaceutical or biomedical industry such as pumps [4], mixers [5] or fans [6].

Cross-flow fans are known for their large length-to-diameter ratios. Due to their rectangular inlet and outlet cross-sections, a uniformly distributed inflow and outflow is produced [7]. Together with a suitable fan housing design, cross-flow fans are implemented in numerous applications ranging from air conditioning devices [8] to sophisticated gas-circulation systems in excimer laser [9]. Gas-discharge excimer laser are for example part of lithography machines, which are required in the manufacturing process of integrated microchips in semiconductor industry [10]. Such lasers need an internal fan that enforces the circulation of the laser gas. The goal is to keep the active medium renewed in the lasing region and to obtain a high flow rate through other components in the chamber [11]. For high-pulse-rate operations a well-designed gas-circulation system is crucial. Therefore, by employing two bearingless motors as the proposed novel cross flow-fan, the aforementioned advantages of extremely long lifetime, low maintenance costs and highly compact motor design
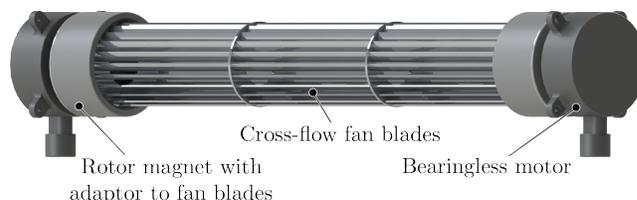
will strongly improve the excimer laser performance. The high safety level of a fully encapsulated and hermetically sealed rotor is emphasized as well, since the process chamber includes potentially harmful excimer gases.

So far, magnetically levitated axial fans have been proposed by several authors. In [12], an axial fan is presented where two passive magnetic bearings stabilize four degrees of freedom (DOFs), radial and tilt directions. The control of the axial direction (5th DOF) is solved using an active magnetic bearing, while the rotational degree of freedom is actuated separately by a permanent magnet synchronous motor. A one-axis (z-direction) actively and four-axes passively positioned axial fan is realized by [13] and [14] as well. However, the axial force and the torque are independently regulated by the q- and d-currents of the single-drive bearingless motor with laminated stator cores. In [6], an axial fan application is suggested using a bearingless axial-force/torque motor. Two radial permanent magnetic ring bearings stabilize radial and tilt deflections of the rotor passively, whereas axial force and drive torque are controlled actively. The proposed motor topology features a bell-shaped exterior rotor with an inner shaft.

The goal of this paper is to introduce the novel bearingless cross-flow fan by means of a prototype. The focus lies on a compact motor that maintains chemical resistance and high purity standards as is desired in gas-circulation systems of excimer laser. **Sec. II** shows the conceptual design of the used motor topology and briefly explains its working principle. Based on two bearingless motors, the cross-flow fan prototype will then be described in **Sec. III**. The system is characterized with pressure-flow curves as well as motor performance measurements on an ISO 5801 based test rig in **Sec. IV**.
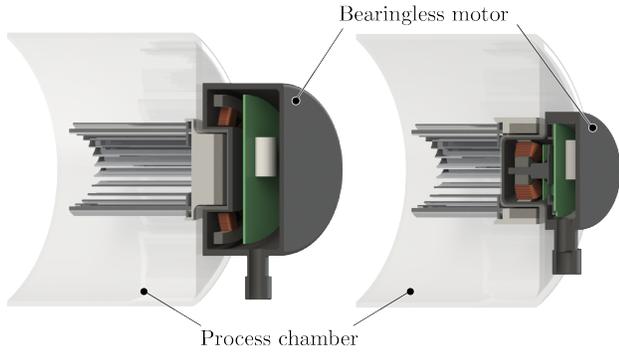
Fig. 2: Conceptual design of a cross-flow fan in a process environment (e.g. excimer laser application) which is driven by bearingless motors. The interior-rotor type (left) requires much larger motor dimensions for all its components than the exterior-rotor design (right). Therefore, the latter is chosen due to the compactness requirements of the target application.

Fig. 3: Conceptual drawing of a bearingless motor with six stator teeth and six corresponding coils. The rotor consists of a back iron ring and four permanent magnets that are magnetized in alternating order.

II. MOTOR TOPOLOGY

Since the focus of this paper lies on the application of a cross-flow fan in excimer lasers, a particularly compact and easily maintainable motor design has to be chosen. To achieve such a system, a reasonable decision between an exterior or interior type of motor is necessary as a first step. **Fig. 2** illustrates two possible concepts, where the left design shows an interior-rotor type (stator surrounding rotor) and the right design, an exterior-rotor type (rotor surrounding stator). As visualized, for an exterior-rotor type the stator together with all the sensors, control and power electronics barely exceeds the diameter of the fan blades, whereas the interior version has much larger dimensions. Therefore, the decision has been made in favor of the highly compact exterior-rotor type design.

In a second step, the number of stator teeth and the pole pair number has to be selected satisfying the compactness criteria as well. To get a functional bearingless motor a minimal stator slot number of four is necessary [15]. However, this topology shows disadvantageous single-phase behavior with large cogging torque [16]. The uneven stator teeth number of five has the drawback of permanently requiring high bearing currents to levitate the rotor [16]. Therefore, a slot number of six offers a promising trade-off between a compact design and a well functioning motor and was chosen for this study [16]. When selecting the rotor pole pair number p for the six-slot design, the condition has to be fulfilled

$$p = 2 + (n \cdot 6), \qquad n = 0, 1, 2, \ldots \tag{1}$$

as described in [16]. The presented rotor satisfies this condition by having four permanent magnets ($p = 2$) that are magnetized in alternating order in radial direction. Finally, **Fig. 3** illustrates the selected motor topology. The stator includes six teeth made of laminated iron with six corresponding copper coils, while the rotor consists of a back iron ring and four permanent magnets. This motor setup can now generate both bearing forces and drive torque, thus stabilize the systems 6 DOFs.
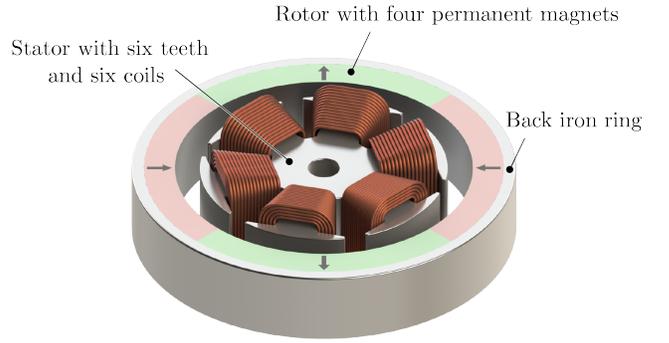
A. Passive Bearing

The term *passive* implies that the generated bearing forces originate solely from the permanent magnets. For the presented topology, the attracting reluctance forces between the stator iron and the rotor magnets act in favor of axial (1 DOF) and tilting (2 DOFs) stability. This means that a distortion from the rotor's center position in axial or tilting direction is counteracted by restoring forces. The extent to which those forces react is defined by the axial force displacement factor

$$k_z = \frac{\Delta F_z}{\Delta e_z} \tag{2}$$

and the torque factor

$$k_\varphi = \frac{\Delta M_\varphi}{\Delta \varphi}. \tag{3}$$

If those factors are sufficiently large, which is the case for this setup, the axial and tilting directions are fully stabilized by passive bearings. Using passive stabilization contributes to achieving a highly compact system as well. However, it is physically impossible to stabilize all DOFs purely passively (Earnshaw's theorem [17]).

B. Active Bearing

When dislocating the rotor from its center position in radial direction, the resulting reluctance force will support that movement until stator and rotor mechanically collide. This destabilizing force can be described by a radial force displacement factor

$$k_{x,y} = \frac{\Delta F_{x,y}}{\Delta e_{x,y}}. \tag{4}$$

Since no stable radial rotor position is possible, an active magnetic bearing has to counteract this destabilizing force in the two DOFs. Such a resulting suspension force can be generated by an air-gap flux-density distribution, having a frequency component of

$$f_{bng} = f_{mech} \cdot (p \pm 1), \tag{5}$$

as described in [18]. Combining a suitable harmonic wave coming from the winding scheme with the harmonics from the

(a) Radial force generation

(b) Torque generation
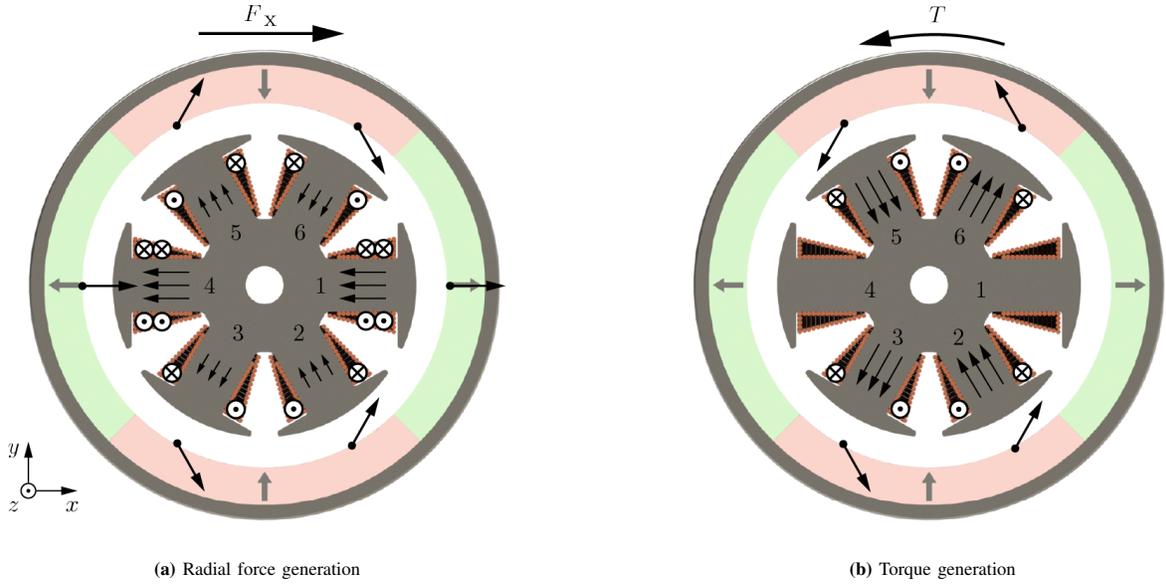
Fig. 4: (a) Radial force generation in x-direction: two opposite coils have currents of same magnitude but opposite direction. Forces in y- direction cancel each other out, so a force F_x results. **(b)** Torque generation: two opposite coils have currents of same magnitude and same direction. Radial forces cancel each other out while tangential forces create a torque T.

stator teeth, these flux-density components can be generated [18]. The resulting suspension forces include radial as well as tangential forces. As shown in **Fig. 4(a)**, a radial force F_x is created when two opposite stator teeth (e.g. coils 1 and 4) have currents of same magnitude but opposite direction. Following this principle, the rotor can be completely stabilized in the two radial DOFs.

C. Torque Generation

The last DOF is the motor torque, which can be created by an air-gap flux-density distribution of

$$f_{\mathrm{drv}} = f_{\mathrm{mech}} \cdot p, \tag{6}$$

as described in [18]. The resulting torque stems from tangential forces while the radial forces cancel each other out. **Fig. 4(b)** illustrates how a torque is created for the proposed system when two opposite stator teeth have currents of same magnitude and same direction.

D. Rotor Control

So far, the active bearing and drive torque have been described as separate entities. However, for combined windings (bearing and drive currents in one coil), these components need to be correctly taken into account within the control system. As can be seen in **Fig. 4(a)** and **Fig. 4(b)**, desired forces can be achieved by a corresponding summation or subtraction. When the sum of drive and bearing currents of the six coils is taken, it results in currents in three non-adjacent coils, whereas subtracting them leads to currents in the remaining three coils [16]. These mathematical operations allow to control bearing forces and drive torque within combined coils by superimposing bearing and drive currents.

E. Combining two Bearingless Motors

For the proposed bearingless cross-flow fan, two such motors are responsible for the active bearing and torque generation of the long-shafted rotor blades. Theoretically, having a double-sided implementation offers twice the available torque for the blade rotation. As explained before, for a bearingless motor with combined windings the drive and bearing functions are handled separately then superimposed. When combining two such motors with a shared rotor, the control scheme has to be adapted. The introduced prototype features a control structure implemented for each motor independently.

III. PROTOTYPE

Fig. 5(a) shows the final cross-flow fan prototype with its dimensions. For the two motors, each stator is cast into a 3D printed housing with a diameter of $d_{\mathrm{M}} = 75\,\mathrm{mm}$. Additionally, a 3D printed adaptor is mounted onto each magnet allowing to mechanically connect the fan blades and creating a common rotor. The fan blades stem from a conventional cross-flow fan having a length of $L = 420\,\mathrm{mm}$ and a diameter of $d_{\mathrm{B}} = 61\,\mathrm{mm}$. The CAD rendering in **Fig. 5(b)** visualizes the internal components of the prototype including the stator iron, copper coils and the integrated power electronics while **Fig. 5(c)** summarizes the technical data of a single motor prototype.

Cross-flow fan performance strongly depends on the flow field, which is heavily influenced by the geometry of casing walls and impeller [19]. There are various numerical as well as experimental studies that try to simulate these flow patterns [20] - [22]. However, no clear design procedure is available since the models lack to fully represent the complex features of the flow field and loss mechanisms [19]. In order to investigate
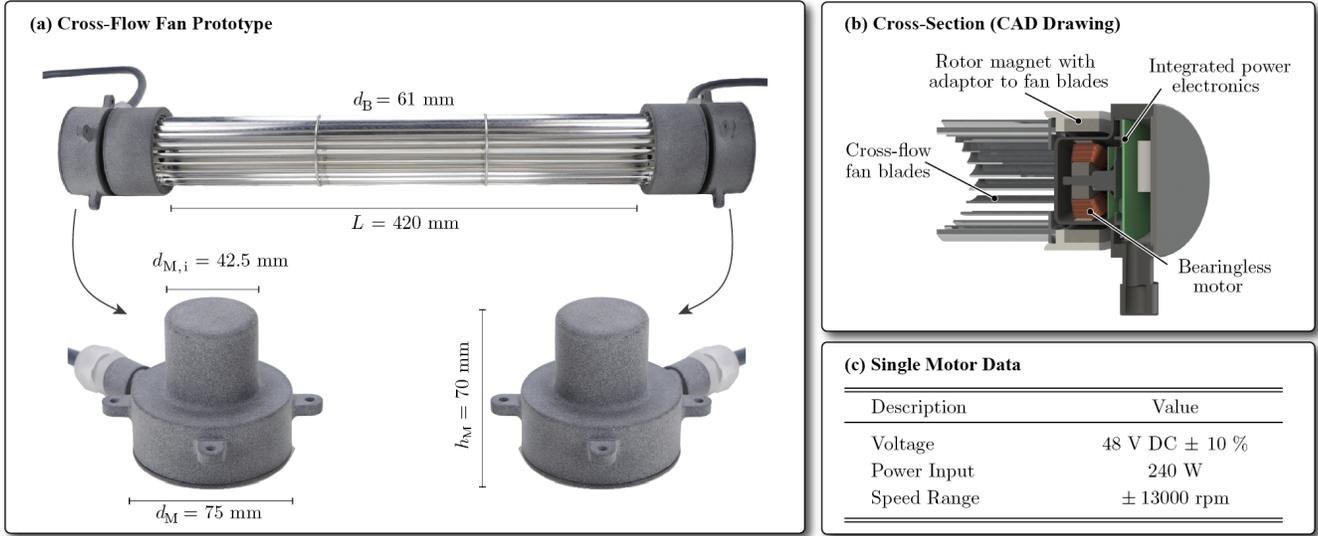
Fig. 5: The bearingless cross-flow fan prototype where **(a)** specifies the dimensions, **(b)** illustrates the internal components with a CAD drawing of the cross section and **(c)** tabulates the technical data of a single motor prototype.

the prototype's functionality, the casing walls have been designed and 3D printed according to a conventional cross-flow fan (cf. **Fig. 6(b)**). Due to the complexity of the fluiddynamical behavior, the casing walls and impeller have not yet been optimized, however, this prototype can now be characterized by means of different performance measurements.

IV. MEASUREMENTS

A. Test Rig

The test rig is based on the ISO 5801 norm, which describes how performance measurements of industrial fans can be performed using standardized airways. As illustrated in **Fig. 6(a)**, it consists of a ducted inlet and ducted outlet ($d_{\text{duct}} = 200\,\text{mm}$) and incorporates different components. A *flow control valve* at the inlet side allows to regulate the flow of the incoming air stream. For the fan characterization, the difference of the total pressures

$$\Delta p_{\text{tot}} = p_{\text{tot, out}} - p_{\text{tot, in}} \tag{7}$$

has to be detected, where the total pressure is equal to the sum of static and dynamic pressure

$$p_{\text{tot}} = p_{\text{stat}} + p_{\text{dyn}}. \tag{8}$$

Since the cross sections of the inlet and outlet duct are equal, the dynamic pressure does not change over the fan ($p_{\text{dyn, in}} = p_{\text{dyn, out}}$) and the total pressure difference becomes

$$\Delta p_{\text{tot}} = p_{\text{stat, out}} - p_{\text{stat, in}}. \tag{9}$$

Therefore, it is possible to measure the static pressure before and after the fan with two *pressure sensors* to get the total pressure difference. The outgoing air stream is detected with a *flow sensor*, where a honeycomb *flow straightener* is required on the inlet side to straighten the air flow. The test rig's dimensions are summarized in **Fig. 6(c)** and the pressure and flow sensor data in **Fig. 6(d)**.

B. Fan Characterization

The pressure-flow curves of the presented cross-flow fan are shown in **Fig. 7** and **Fig. 8**, where the former illustrates the physical values (p and Q) and the latter the dimensionless parameters (φ and Ψ). The dimensionless flow number φ is defined as

$$\varphi = \frac{Q}{u \cdot d_B \cdot L}, \tag{10}$$

where d_B and L are the blades' diameter and length and u is the velocity of circulation

$$u = \pi \cdot d_B \cdot n \tag{11}$$

with n being the rotor speed. The dimensionless pressure number Ψ is defined as

$$\Psi = \frac{\Delta p_{\text{tot}}}{\rho_{\text{air}}/2 \cdot u^2}, \tag{12}$$

with a density of air being $\rho_{\text{air}} = 1.2041\,\text{kg/m}^3$. The measurements have been conducted with rotor speeds of $2000\,\text{rpm}$, $2500\,\text{rpm}$, $3000\,\text{rpm}$ and $3500\,\text{rpm}$. As expected, the pressure difference over the fan Δp_{tot} decreases with increasing flow rate Q (cf. **Fig. 7**). The low pressure values are characteristic for cross-flow fans, since they are intended for applications where uniformly distributed outflows are desired rather than high pressures. Looking at the dimensionless parameters in **Fig. 8**, an unexpected parallel shift between the different speeds is noticed. Although the curves should overlap in the dimensionless plot, the pressure and flow coefficients seem to decrease with increasing speeds. This might be explained by rotordynamical effects that occur for long-shafted rotors. These vibrations start to aggravate the stabilization by means of magnetic bearings and lower the performance of the fan in terms of pressure and flow. Appropriate measures will have to be studied in detail and correctly implemented.
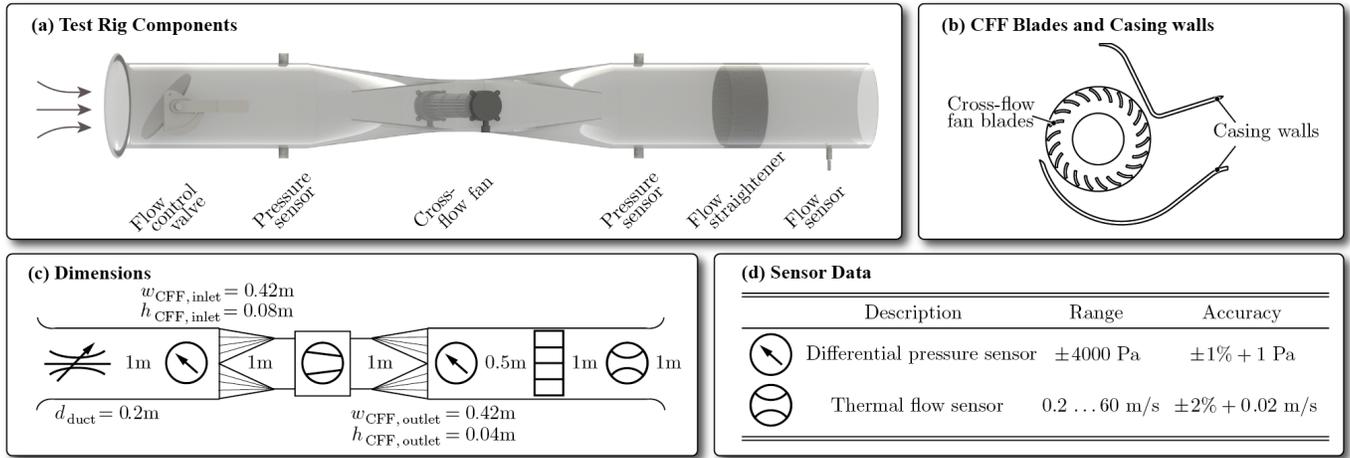
Fig. 6: Conceptual drawing of the ISO 5801 based test rig where **(a)** visualizes its components including the cross-flow fan (CFF) prototype, a flow control valve, two pressure sensors, a flow straightener and a flow sensor, **(b)** shows a sketch of the CFF blades and casing walls, **(c)** the test rig's dimensions and **(d)** tabulates the technical data of the pressure and flow sensors.

C. Motor Performance

Fig. 9 shows the drive currents of the unilaterally driving motor M_1 and **Fig. 10** the bearing currents of motors M_1 and M_2. These figures prove that the novel cross-flow fan prototype has been successfully commissioned up to $3500\,\text{rpm}$. The drive currents (cf. **Fig. 9**) allow further important conclusions regarding the prototype's performance potential. The mechanical power P_{mech} of a rotational system is defined as

$$P_{\text{mech}} = T \cdot \omega = I_{\text{drv}} \cdot k_{\text{M}} \cdot 2\pi n, \tag{13}$$

with T being the torque, ω the angular velocity and k_{M} the torque constant. Therefore, it follows that

$$P_{\text{mech}} \propto I_{\text{drv}} \cdot n. \tag{14}$$

The hydraulic power P_{hyd} is defined as

$$P_{\text{hyd}} = \Delta p \cdot Q. \tag{15}$$

Since $\Delta p \propto n^2$ and $Q \propto n$, it follows that

$$P_{\text{hyd}} \propto n^3. \tag{16}$$

Finally, since $P_{\text{mech}} \propto P_{\text{hyd}}$ following proportionality results:

$$n \propto \sqrt{I_{\text{drv}}}. \tag{17}$$

For the proposed prototype with an empirical drive current limit of $I_{\text{drv,max}} = 4\text{A}$ (for each motor), an extrapolation with relation (17) results in a theoretically achievable rotor speed of $n_{\text{pot}} \approx 6400\,\text{rpm}$. This should point out that the currently reached speed of $3500\,\text{rpm}$ has not exploited the motor's full mechanical power yet.

However, analyzing the bearing currents (cf. **Fig. 10**) an increase with increasing speed is noticed while large fluctuations start to occur at $3500\,\text{rpm}$. Like previously mentioned, rotordynamical effects start to destabilize the system, thus present a new challenge for double-sided bearingless motor applications with long shafts. These phenomena will have to be studied in detail and counteracting measures implemented.
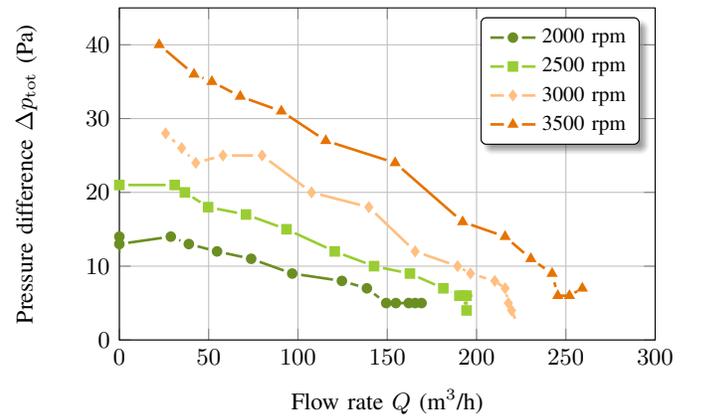
Fig. 7: Pressure-flow characteristics of the proposed bearingless cross-flow fan prototype, where measurements are performed for different rotor speeds.
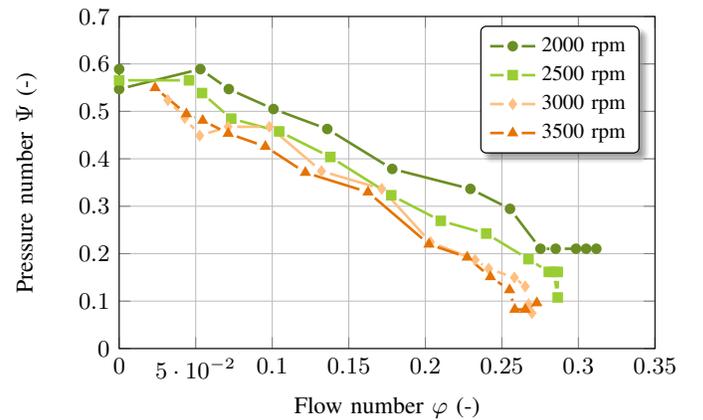
Fig. 8: Dimensionless pressure-flow characteristics of the proposed bearingless cross-flow fan prototype, where the dimensionless parameters are calculated according to (10) and (12).
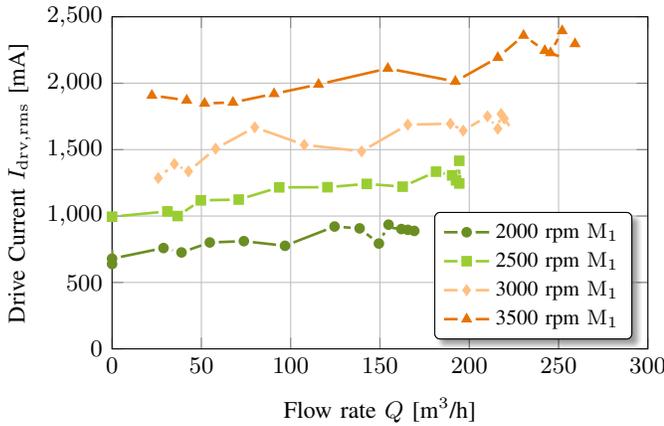
Fig. 9: Drive currents of the unilaterally driving motor M_1.
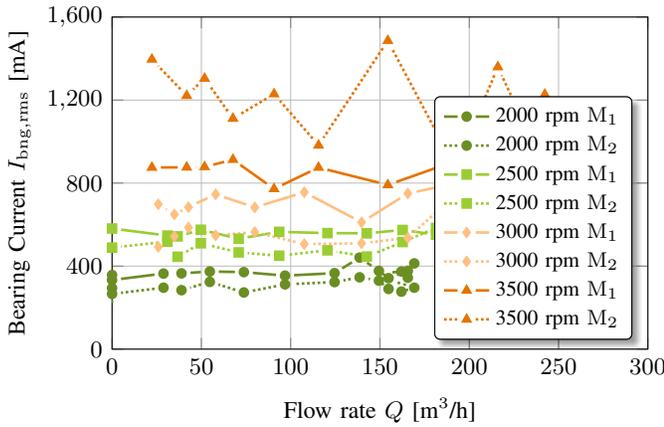
Fig. 10: Bearing currents of motors M_1 and M_2, where M_1 is the unilaterally driving motor.

V. CONCLUSION

The novel bearingless cross-flow fan has been introduced in this paper. Based on two bearingless motors, its working principle has been described featuring unique performance in an ultra compact design. Its chemical resistance and high purity attributes are ideal for demanding applications such as gas-circulation systems in excimer laser. A prototype has been built and corresponding pressure-flow measurements performed on an ISO 5801 based test rig. Rotor speeds of up to $3500\,\mathrm{rpm}$ have been reached and air flows up to $250\,\mathrm{m^3/h}$ achieved.

However, the available torque of the two bearingless motors has not been fully exploited yet, since rotordynamical effects start to interfere with the stabilization of the long rotor. Future work will focus on detecting these vibrations as well as implementing appropriate counter-measures within the control system such that maximum rotor speeds can be achieved.

ACKNOWLEDGMENT

REFERENCES

[1] X. Sun, L. Chen, and Z. Yang, "Overview of bearingless permanent-magnet synchronous motors," *IEEE Transactions on Industrial Electronics*, vol. 60, no. 12, pp. 5528-5538, December 2013.

[2] T. Nussbaumer, P. Karutz, F. Zurcher, and J. W. Kolar, "Magnetically levitated slice motors - An overview," *IEEE Transactions on Industry Applications*, vol. 47, no. 2, pp. 754-766, March/April 2011.

[3] T. Holenstein, T. Nussbaumer, and J. W. Kolar, "A bearingless synchronous reluctance slice motor with rotor flux barriers," *2018 International Power Electronics Conference*, Niigata, 2018, pp. 3619-3626.

[4] T. Nussbaumer, K. Raggl, P. Boesch, and J. W. Kolar, "Trends in integration for magnetically levitated pump systems," *2007 Power Conversion Conference-Nagoya*, Nagoya, 2007, pp. 1551-1558.

[5] B. Warberger, R. Kaelin, T. Nussbaumer, and J. W. Kolar, "50-N·m/2500-W Bearingless motor for high-purity pharmaceutical mixing," *IEEE Transactions on Industrial Electronics*, vol. 59, no. 5, pp. 2236-2247, May 2012.

[6] W. Gruber, W. Bauer, D. Wetsch, B. Klammer, and N. Kurita, "Implementation of a bearingless axial-force/torque motor fan with flex-PCB windings," *2019 IEEE International Electric Machines & Drives Conference (IEMDC)*, San Diego, 2019, pp. 179-184.

[7] T. Q. Dang, and P. R. Bushnell, "Aerodynamics of cross-flow fans and their application to aircraft propulsion and flow control," *Progress in Aerospace Sciences*, vol. 45, no. 1-3, pp. 1-29, 2019.

[8] YC. Shih, HC. Hou, and H. Chiang, "On similitude of the cross flow fan in a split-type air-conditioner," *Applied Thermal Engineering*, vol. 28, no. 14-15, pp. 1853-1864, 2008.

[9] J. J. Ewing, "Excimer laser technology development," *IEEE Journal of selected topics in quantum electronics*, vol. 6, no. 6, pp. 1061-1071, 2000.

[10] D. Basting, K. Pippert, and U. Stamm, "History and future prospects of excimer lasers," *Sec. Int. Symposium on Laser Precision Microfabrication*, Int. Society for Optics and Photonics, vol. 4426, pp. 25-34, 2002.

[11] R. Delmdahl, and R. Pätzel, "Excimer laser technology trends," *Journal of Physics D: Applied Physics*, vol. 47, no. 3, p. 034004, 2013.

[12] G. Jungmayr, E. Marth, M. Panholzer, W. Amrhein, F. Jeske, and M. Reisinger, "Design of a highly reliable fan with magnetic bearings," *Proceedings of the Institution of Mechanical Engineers, Part I: Journal of Systems and Control Engineering*, vol 230, no. 4, pp. 361-369, 2016.

[13] H. Sugimoto, I. Shimura, and A. Chiba, "A novel stator structure for active axial force improvement in a one-axis actively positioned single-drive bearingless motor," *IEEE Transactions on Industry Applications*, vol. 53, no. 5, pp. 4414-4421, Sept./Oct. 2017.

[14] H. Sugimoto, I. Shimura, and A. Chiba, "Principle and test results of energy-saving effect of a single-drive bearingless motor in cooling fan applications," *IEEJ Journal of Industry Applications*, vol. 6, no. 6, pp. 456-462, 2017.

[15] T. Reichert, T. Nussbaumer, W. Gruber, and J. W. Kolar, "Bearingless permanent-magnet motor with 4/12 slot-pole ratio for bioreactor stirring applications," *IEEE/ASME Transactions on Mechatronics*, vol. 16, no. 3, pp. 431-439, June 2011.

[16] T. Reichert, T. Nussbaumer, and J. W. Kolar, "Bearingless 300-W PMSM for bioreactor mixing," *IEEE Transactions on Industry Applications*, vol. 59, no. 3, pp. 1376-1388, March 2012.

[17] S. Earnshaw, "On the nature of the molecular forces which regulate the constitution of the luminiferous ether," *Transactions of the Cambridge Philosophical Society*, vol. 7, pp. 97-112, 1842.

[18] F. Zürcher, T. Nussbaumer, and J. W. Kolar, "Principles of magnetic levitation and motor torque generation by superposition of harmonics in bearingless brushless motors," in *Proc. 35th IEEE IECON*, Nov. 2009, pp. 1246-1251.

[19] A. Toffolo, "On the theoretical link between design parameters and performance in cross-flow fans: a numerical and experimental study," *Computers & Fluids*, vol. 34, no. 1, pp. 49-66, 2005.

[20] L. Casarsa, and P. Giannattasio, "Experimental study of the three-dimensional flow field in cross-flow fans," *Experimental thermal and fluid science*, vol. 35, no. 6, pp. 948-959, 2011.

[21] Ö. Özer, and d. Kumlutaş, "Experimental investigation on cross flow fan's casing parameters inside of a split air conditioner indoor unit by Stereo Particle Image Velocimetry," *Applied Thermal Engineering*, vol. 124, pp. 1233-1246, 2017.

[22] A. Ciocanea, A. Marin, and D. L. Buretea, "The influence of housing on the internal flow of a cross flow fan impeller," *2019 International Conference on Energy and Environment (CIEM)*, Oct. 2019, pp. 464-468.